Electron capture and ionization processes in high-velocity Cn+ , C–Ar and Cn+ , C–He collisions

G Labaigt, A Jorge, C Illescas, K Béroff, Alain Dubois, B Pons, M Chabot

Electron capture and ionization processes in high-velocity C_n^+, C - Ar and He collisions

G. Labaigt[1,2], A. Jorge[3], C. Illescas[3], K. Béroff[4], A. Dubois[1,2], B. Pons[5] and M. Chabot[6]

[1] Sorbonne Universités, UPMC Univ Paris 06, UMR 7614, Laboratoire de Chimie Physique-Matière et Rayonnement, F-75231, Paris, France

[2] CNRS, UMR 7614, LCPMR, 75005, Paris, France

[3] Departamento de Química C-IX, Universidad Autónoma de Madrid, 28049 Madrid, Spain

[4] Institut des Sciences Moléculaires d'Orsay, CNRS and Université Paris-Sud, F-91405 Orsay Cedex, France

[5] CELIA, Univ. Bordeaux – CNRS UMR 5107 – CEA, 351 Cours de la Libération, 33405 Talence, France

[6] Institut de Physique Nucléaire d'Orsay, CNRS and Université Paris-Sud, F-91406 Orsay Cedex, France

E-mail: karine.beroff@u-psud.fr, alain.dubois@upmc.fr, pons@celia.u-bordeaux1.fr

Abstract. Single and double electron capture as well as projectile single and multiple ionization processes in 125 keV/u C_n^+ - He (n=1-5) and C_n^+-Ar (n=1,2,4) collisions have been studied experimentally and theoretically. Helium target single and double ionization cross sections are also reported for C_n^+ - He (n=1,4) collisions in the 100-400 keV/u impact energy domain. These results are compared with predictions from the Independent Atom and Electron (IAE) model developed to describe cluster-atom collisions. The ion/atom-atom probabilities required for the IAE simulations have been determined by Classical Trajectory Monte Carlo (CTMC) and SemiClassical Atomic Orbital Close-Coupling (SCAOCC) calculations for the Ar and He targets, respectively. For comparison electron capture cross sections were also measured in C - He and Ar collisions. In general the agreement between experiment and IAE calculations has been found rather good with the exception of double electron capture leading to anionic C_n^- species.

PACS numbers: 36.40.-c, 34.10.+x, 34.50.Gb, 34.70.+e, 36.40.Qv

1. Introduction

Collisions between polyatomic systems (clusters, molecules) and atoms or ions have been intensively studied for the last twenty years. Studies involving metallic [1, 2, 3], covalent [4, 5], and molecular [6, 7, 8] clusters have been reported as well as collisions with large molecules of biological [9, 10] or astrophysical [11, 12] interest. In these works, emphasis has mainly been put onto the relaxation of the excited polyatomic system and the collisional process in itself has been relatively less studied: comparisons between measured and calculated cross sections remain therefore scarce in the literature. We may cite the electron capture process in low-velocity collisions [13, 14] in which a simplified representation of the cluster was performed. The ionization of simple molecules (such as H_2 and H_2O) in high-energy collisions also retained attention and motivated strong experimental and theoretical efforts [15, 16, 17, 18]. Experimental and theoretical studies on ionization of larger molecules are in progress [19]. By contrast the electron capture process in high-velocity collisions has received little attention and this is particularly true for the case of double electron capture.

In this paper, we present a joint experimental and theoretical study of electron capture and ionization processes in carbon clusters - He and Ar collisions at high impact velocity v. More precisely, single and double electron capture cross sections, as well as single and multiple projectile ionization cross sections, have been measured in $C^+_{n=1-5}$-He, Ar collisions at 125 keV/amu impact energy (v = 2.25 a.u.). Moreover, single electron capture cross sections in C - He, Ar collisions have been measured, with the aim to check the reliability of the probabilities underlying the modelling of C^+_n - He, Ar collisions. The present work thus significantly improves a recent study on C^+_n-He collisions [20], in which we focused on the anionic production $C^+_n + He \rightarrow [C^-_n] + He^{++}$ ‡. We indeed complete the description of $C^+_n + He$ collisions by reporting the cross sections for projectile and target ionizations. Furthermore we present results obtained with a different target atom, which allows us to study the dependence of the collisional processes upon target atomic number. For the electronic processes considered, our experimental set-up gives access to the dissociation branching ratios which are presented herein for neutral and anionic species.

An *ab initio* description of C^+_n-He, Ar collisions remains beyond present capabilities, because of the multielectronic nature of both the target and the projectile, combined with the complex nuclear degrees of freedom of the impinging clusters. We thus had recourse to the Independent Atom and Electron (IAE) model to describe the C^+_n-He, Ar collisions: IAE is a collision model where the cluster is assumed to be made of independent atoms in which electrons move independently. Cluster-atom collisions are thus described in terms of combinatorial products of inclusive one-electron probabilities involving each atomic or ionic constituent of the cluster. The IAE approach has initially be introduced to predict multi-ionization of molecules [21] and was successfully employed

‡ The notation $[C_n]$, which will be employed throughout the present paper, indicates that the C_n species can be found in their non-dissociative or dissociative (e.g. $C_p + C_{n-p}$) forms.

to describe ionization of C_n^+ clusters [5, 22]. The applicability of the IAE model is obviously conditioned by the availability of the one-electron ion-atom and atom-atom underlying probabilities. As it was shown in our recent study of electron capture in C_n^+-He collisions [20] this can be problematic since electron capture probabilities between neutral species (C and He) are generally unknown while playing an important role in the dynamics of the clusters. In [20] we circumvented this problem by defining the charge exchange C-He probability as a scaled C^+-He probability. In the present work we decide to get rid of such a scaling and accordingly performed state-of-the-art calculations of all capture and ionization probabilities in the C,C^+ - He, Ar collisions that underly the IAE simulations. These calculations were performed by means of the Classical Trajectory Monte Carlo (CTMC) method for C^+,C-Ar collisions while the Semi-Classical Atomic Orbital Close Coupling (SCAOCC) was employed for C^+,C-He collisions. The one active-electron CTMC method is a quite standard approach which is known to provide accurate results for electron capture and target ionization from intermediate to high impact energies [23, 24, 25]. Its two active-electron version, with one active electron on each colliding center, has been successfully applied to model target and projectile ion formation in H-H collisions [26, 27]. We are thus confident that implementations of these approaches will provide reliable results for the same processes in the present high-energy C^+,C-Ar cases. On the other hand, SCAOCC is a well-established approach to provide accurate cross sections for capture, excitation and ionization in many fundamental systems [23, 28, 29]. Furthermore, even though the IAE model is based on the use of inclusive one-electron probabilities, various implementations of the SCAOCC scheme have been run herein, with increasing number of active electrons. This strategy was important to test the accuracy of some approximations – in particular the Independent Particle Model (IPM) for the helium target – and also to check whether the range of impact parameters, of importance for the IAE implementation, for electron capture by C^+ and C projectiles depends on the level of sophistication of the calculations.

The organization of the paper is as follows. Section 2 is devoted to the presentation of the experimental set-up, focusing on its features important for the interpretation of the data. In section 3 we outline the IAE, CTMC and SCAOCC treatments, transferring the details of the models to the appendices. Our results are presented and discussed in section 4, paying particular attention to the detailed comparison between experimental and theoretical cross sections. Conclusions are given in section 5.

Atomic units are used unless otherwise stated.

2. Experiment

The set-up has been presented in detail in [20] so that we only outline it here. Experiments were conducted at the Tandem accelerator in Orsay (France) with beams of hot § carbon clusters C_n^+ of velocity 2.25 a.u. Collisions between projectiles and atoms

§ Mean thermal energies were 2 or 3 eV depending on n [22]. An unknown contribution of metastable electronic states for the C^+ beam was possibly present.

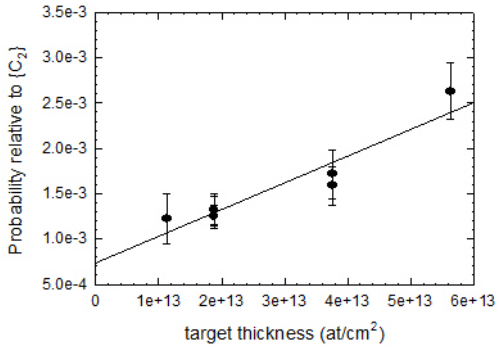

Figure 1. Target thickness dependence of the C^-/C^{q+} production (q$\geq$ 1) relative to the $[C_2]$ one in C_2^++Ar collisions. The solid line is a linear regression to the experimental points; its slope is used to extract the electron capture cross section onto C in the C-Ar collision.

occurred in a gaseous jet (argon or helium) of known thickness. The thickness was varied by changing the flow rate through the jet capillary. Fragments produced in the collisions were deflected according to their charge over mass ratios by an electrostatic analyser situated 325mm (70 ns) after the jet. After deflection the fragments stopped into several solid-state silicon detectors positioned as to cover the whole emission solid angle (4π in the projectile's frame). Analysis of the detector transient currents allowed to extract the mass and charge of each fragment impinging on it. In the experiment with the argon target, only detectors for neutral and negatively charged fragments were used (positive fragments were detected in a separate experiment by changing the electric field polarity) whereas in the case of the helium target, fragments of all neutral, positive and negative charges were detected in coincidence. In experiments performed at slightly different velocities (v=2, 2.6, 4 a.u) the He recoil charge state was recorded in coincidence with positive and neutral fragments. This allowed us to disentangle the pure ionization and capture processes responsible for the charged helium production; method and details are given in [30].

As explained in [20] the electron capture onto neutral C_n occurs in a second collision subsequent to single electron capture onto the incident C_n^+ projectile. As a consequence it was extracted by a target thickness dependence of the anionic production probability. We measured the electron capture process onto the neutral C atom in the C-Ar collision from the target thickness dependence of the C^-/C^{q+} ($q \geq 1$) production in the C_2^+-Ar collision (see figure 1). Indeed this production relates to the electron capture cross section in a simple way (see equations (6) and (7) in [20] with $n = 2$ and $p = 1$). Further, we investigated a possible depopulation of the C^-/C^{q+} channels by electron detachment from C^- [31] in a third collision but we found that this contribution is negligible. For incident C^+ and C_4^+ projectiles we worked at a fixed (small) target thickness (respectively 1.65 10^{13} at/cm^2 and 1.51 10^{13} at/cm^2 for C^+ and C_4^+). We calculated at theses thicknesses the percentage of double collisions contributing to the

Table 1. Measured branching ratios (BR) for relaxation of excited C_n produced in C_n^+-He,Ar collisions at v=2.25 a.u; $n = 2$ to $n = 4$ from top to bottom.

Channel	BR (rel.error) (He)	BR (rel.error) (Ar)
C_2 (intact)	0.46(2%)	0.42(2%)
C/C	0.54(2%)	0.58(2%)
C_3 (intact)	0.44(2%)	
C_2/C	0.48(2%)	
3C	0.08(3%)	
C_4 (intact)	0.19(2%)	0.19(10%)
C_3/C	0.51(2%)	0.48(8%)
C_2/C_2	0.21(3%)	0.17(23%)
C_2/2C	0.07(9%)	0.13(15%)
4C	0.02(10%)	0.03(30%)

production of anionic C_n^- and subtracted the associated contributions (respectively 2(±0.5)% and 15(±5)% for n=1 and 4) in order to derive the double electron capture cross section.

Cross sections for all electronic processes involving clusters (excitation and ionization, neutralization, anionic production) were obtained by summing probabilities of relaxation channels. For instance, neutralization was obtained by summing relaxation channels involving neutral fragments only. We present in Table 1 the list of relaxation channels of C_n species with their measured branching ratios (BR, which are relative probabilities whose sum, for each n, is normalized to 1). Results with the helium target are close from those obtained at slightly different collision velocities (v =2.6 u.a [32] and 4.5 a.u [33]). This indicates that the internal energies of the clusters after the collision, whose dissociation BR are a signature of [34], are almost independent of v in the range 2-5 a.u. There is neither visible effect associated to the target atomic number since the BR measured in $C_n^+ + Ar$ collision are close to those obtained in the $C_n^+ + He$ collision. This is also the case for the BR associated to the relaxation of anionic clusters presented in Table 2. For these negatively charged clusters we see that BR for intact (non dissociative) relaxation are larger than in the case of neutral clusters. This could be due to the opening of a new relaxation channel in anionic species, namely, electron emission, since this channel is expected to relax C_n^- species much more efficiently than dissociation (see figure 10 in [20]). Our set-up does not give access to this supplementary relaxation channel.

3. Theoretical description

3.1. The Independent Atom and Electron (IAE) model

The dynamics of cluster-atom collisions are described in the framework of the impact parameter approximation [23] in which the projectile, whose center of mass is characterized by the impact parameter **b** with respect to the target, follows rectilinear

Table 2. Same legend as Table 1 for relaxation of C_n^- species and n=2,4; value with an asterisk refers to the sum of BR for C_2^-/C_2 and $C_2^-/2C$ channels.

Channel	BR (rel.error) (He)	BR (rel.error) (Ar)
C_2^- (intact)	0.91(5%)	0.75(17%)
C^-/C	0.09(50%)	0.25(48%)
C_4^- (intact)	0.61(8%)	0.65(31%)
C_2^-/C_2	0.29(20%)	
		0.35* (57%)
$C_2^-/2C$	0.10(100%)	

trajectories with constant velocity **v**. Further we employ the so-called Independent Atom and Electron (IAE) model [20, 5] where all atoms and electrons are treated as independent. For instance, C_n^+ in its equilibrium geometry is modelled as a C^+ ion surrounded by (n-1) independent C neutral atoms. The IAE probabilities thus consist of products of atomic probabilities. For instance the He-induced neutralization probability of a C_n^+ cluster is expressed as:

$$P_{C_n^+ \to C_n}(\mathbf{b}) = \sum_{i=1}^{n} P_{\rm capt}^{(1)}(b_i) \prod_{i=1}^{n}(1 - P_{\rm ion}(b_i)) \prod_{j\neq i}(1 - P_{\rm capt}(b_j)) \qquad (1)$$
$$+ \left[\sum_{i=1}^{n} P_{\rm capt}^{(2)}(b_i) + \sum_{i=1}^{n}\sum_{j>i} 2P_{\rm capt}^{(1)}(b_i)P_{\rm capt}^{(1)}(b_j)\right] \left[\sum_{i=1}^{n} P_{\rm ion}^{(1)}(b_i) \prod_{j\neq i}(1 - P_{\rm ion}(b_j))\right]$$

where b_i marks the impact parameter of the ith center with respect to the target, $P_{\rm capt}^{(1)}(b_i)$, $P_{\rm capt}^{(2)}(b_i)$ and $P_{\rm capt}(b_i)$ stand for single, double, and total electron capture probabilities onto center i and $P_{\rm ion}^{(1)}(b_i)$ and $P_{\rm ion}(b_i)$ stand for projectile single and total ionization probabilities of center i (C or C^+). The first term of eq. (1) represents the dominant contribution to the neutralization probability, which is single electron capture without projectile ionization, described in the (1-P_{ion}) terms. The second term, amounting to a few % at most, corresponds to double electron capture concomitant with projectile single ionization.

The atomic probabilities of processes occuring in C-He and C^+-He collisions are computed assuming the independence of the electrons, *i*.e. in the framework of the well-known Independent Particle Model (IPM, [23, 35, 36]). Furthermore, only valence electrons of the projectile and/or the target are assumed to be active within the dynamics. The probabilities entering eq. (1) can thus be written as:

$$P_{\rm capt}^{(1)}(b_i) = 2p_{\rm c}(b_i)(1 - p_{\rm c}(b_i)) \qquad (2)$$

$$P_{\rm capt}^{(2)}(b_i) = p_{\rm c}(b_i)^2 \qquad (3)$$

$$1 - P_{\rm capt}(b_i) = (1 - p_{\rm c}(b_i))^2 \qquad (4)$$

while

$$P_{\rm ion}^{(1)}(b_i) = 2p_{\rm ion}^{(2s)}(b_i)(1 - p_{\rm ion}^{(2s)}(b_i))(1 - p_{\rm ion}^{(2p)}(b_i))^a + ap_{\rm ion}^{(2p)}(b_i)(1 - p_{\rm ion}^{(2p)}(b_i))^{(a-1)}(1 - p_{\rm ion}^{(2s)}(b_i))^2 \qquad (5)$$

$$1 - P_{\rm ion}(b_i) = (1 - p_{\rm ion}^{(2s)}(b_i))^2 (1 - p_{\rm ion}^{(2p)}(b_i))^a. \quad (6)$$

In (2)-(6), p_c is the probability to capture an electron from He, while $p_{\rm ion}^{(2s,2p)}$ refers to the probability to ionize one electron from the $2s$ and $2p$ valence subshells of C (or C^+). Depending on the projectile (C or C^+), $a = 2$ or 1 in (5)-(6), respectively.

Absolute cross sections are derived by integrating over **b** IAE probabilities such as (1). Since individual b_i depend not only on **b** but also on the cluster orientation [5], we perform an average over all equally probable cluster orientations (θ, φ in spherical coordinates) following eq. (7):

$$\sigma = \frac{1}{4\pi} \int_0^{2\pi} d\varphi \int_0^{\pi} \sin(\theta) d\theta \int P(\mathbf{b}, \theta, \varphi) d\mathbf{b}. \quad (7)$$

Furthermore, a statistical average over the location of the charged center within the cluster is made, and the resulting cross section directly compared against experiment.

We now present the strategy used to compute the one-electron atomic probabilities in C^+,C-Ar and C^+,C-He collisions which are the basic ingredients of the IAE model.

3.2. Classical Trajectory Monte Carlo (CTMC) calculations of one-electron probabilities in C^+,C-Ar collisions

The one-electron probability p_c for charge transfer from Ar to C^+ (or C) is computed under the assumption that only one 3p electron of Ar is active. This is a valuable assumption in the impact energy range considered in the present work [37]. The classical electronic Hamiltonian describing the C^+-Ar collisional system is:

$$H_{1e} = \frac{p^2}{2} + V_{mod}^{(Ar^+ + e)}(r_T) + V_{mod}^{(C^+ + e)}(r_P) \quad (8)$$

while for C-Ar,

$$H_{1e} = \frac{p^2}{2} + V_{mod}^{(Ar^+ + e)}(r_T) + V_{mod}^{(C + e)}(r_P) \quad (9)$$

where p is the momentum of the active electron with respect to the target which is chosen as the origin of the Galilean frame. r_T is the electron-target distance and $r_P = |\mathbf{r}_T - \mathbf{R}|$ is the electron-projectile distance, with $\mathbf{R} = \mathbf{b} + \mathbf{v}t$ in the impact parameter approach. The potential terms $V_{mod}^{(Ar^+ + e)}$ and $V_{mod}^{(C^+, C + e)}$ describe the interactions of the active electron with the target and projectile cores which remain frozen throughout the collision. These so-called model potentials are detailed in Appendix A. Basically they are parametric potentials which are optimized to reproduce as accurately as possible the valence state energies of the target and the projectile.

Besides electron capture, the Hamiltonians (8) and (9) are amenable to the description of target ionization through ejection of the active Ar($3p$) electron. Nevertheless they do not allow to represent the dynamics of the frozen projectile electrons. We could derive effective one-electron Hamiltonians similar to (8)-(9) to obtain the projectile ionization probabilities $p_{\rm ion}^{(2s,2p)}$ required by the IAE simulations. The active electron would belong to either the $2s$ or $2p$ subshell of C^+ (or C) and

all remaining electrons would be frozen. However this would imply to define a model potential for such an unstable system as (Ar+e)≡Ar$^-$. We preferred to switch to an alternative approach where both the $3p$ electron of Ar and one electron of the $n = 2$ shell of C^+ (or C) are active. Collisions involving $2s$ and $2p$ carbon subshells have been explicitly (and separately) considered. The two-active electron Hamiltonian is

$$H_{2e} = \frac{p_1^2}{2} + V_{mod}^{(Ar^+ + e)}(r_{1T}) + V_{mod}^{(C^{2+} + e)}(r_{1P}) + \frac{p_2^2}{2} + V_{mod}^{(Ar^+ + e)}(r_{2T}) + V_{mod}^{(C^{2+} + e)}(r_{2P}) + \frac{1}{|\mathbf{r}_{1T} - \mathbf{r}_{2T}|} \tag{10}$$

for C^+-Ar and, alternatively,

$$H_{2e} = \frac{p_1^2}{2} + V_{mod}^{(Ar^+ + e)}(r_{1T}) + V_{mod}^{(C^+ + e)}(r_{1P}) + \frac{p_2^2}{2} + V_{mod}^{(Ar^+ + e)}(r_{2T}) + V_{mod}^{(C^+ + e)}(r_{2P}) + \frac{1}{|\mathbf{r}_{1T} - \mathbf{r}_{2T}|} \tag{11}$$

for C-Ar, where the indices 1 and 2 in $r_{T,P}$ obviously refer to the two active electrons.

For a given nuclear trajectory (v, b), the electron dynamics have been resolved using the Classical Trajectory Monte Carlo (CTMC) approach to atomic collisions [38]. We employ a classical phase space distribution ρ discretized in terms of N independent trajectories. The Liouville equation, $\frac{\partial \rho}{\partial t} = -\{\rho, H_{(1e,2e)}\}$, which is the classical analogue to the time-dependent Schrödinger equation, then transforms into the well known Hamilton equations monitoring the time evolution of each electron trajectory. Integration of these equations is performed up to the end of the collision, approximated by $t_{end} = 500v^{-1}$, where energy criteria are applied to disentangle capture, excitation and ionization processes [38, 24, 25].

In the case of one active electron, the initial distribution $\rho(\mathbf{r}_1, \mathbf{p}_1, t \to -\infty)$ consists of either a microcanonical $\rho_{Ar}(\mathbf{r}_1, \mathbf{p}_1)$ [39] or (Wigner-like) improved $\rho_{Ar}^{(W)}(\mathbf{r}_1, \mathbf{p}_1)$ [40, 41] sets. In the impact energy range considered in the present work, both sets lead to almost undistinguishable probabilities, consistently with what has already been obtained for simpler collisional systems [25, 41]. It is worth noting that some electron trajectories ends up at t_{end} with energies that quantum mechanically correspond to occupied inner shells of Ar or C^+,C atoms [42]. In such cases, these trajectories are removed from the statistics and the probabilities are accordingly renormalized.

In the case of two active electrons, the initial distribution $\rho(\mathbf{r}_1, \mathbf{r}_2, \mathbf{p}_1, \mathbf{p}_2, t \to -\infty)$ consists of the product of microcanonical sets $\rho_{Ar}(\mathbf{r}_1, \mathbf{p}_1)\rho_{C^+,C}(\mathbf{r}_2, \mathbf{p}_2)$ of dimension $N = N_{Ar}N_{C^+,C}$ [26, 27]. Integration of the Hamilton equations is performed for the $N_{Ar}N_{C^+,C}$ pairs of electrons. In this framework, modelling a capture process inevitably leads to autoionization because of the electrostatic repulsion between two active electrons located on the same nuclear center [43]. This results in a contamination of the genuine single ionization processes, which has been found to be small (1-3%). Note that the projectile ionization probabilities $p_{\rm ion}^{(2s,2p)}$ are inclusive, *i.e.* they are calculated irrespectively of the final target state.

3.3. Semiclassical Atomic Orbital Close-Coupling (SCAOCC) calculations for C^+,C-He collisions

For C^+,C-He collisions, atomic probabilities have been obtained by means of SCAOCC calculations. This approach used in the present work has previously been described in e.g. [23, 44, 45], so that we only outline here the main features of the method and of its implementations to deal with the two collision systems under consideration. In the semiclassical approximation we obtain the scattering wavefunction ψ by solving non perturbatively the time dependent Schrödinger equation:

$$\left[H_e - i\frac{\partial}{\partial t}\right] \psi(\vec{r_1}, \vec{r_2}, ...\vec{r}_{n_e}, t) = 0 \tag{12}$$

for an electronic Hamiltonian H_e where n_e active electrons are taken into account. The wavefunction is accordingly expanded on a set of electronic states described with Gaussian Type Orbitals (GTO) and spin-adapted products of these GTOs centered on both isolated collision partners. Furthermore they are augmented by plane-wave electronic translation factors to cancel spurious dipolar couplings and to ensure Galilean invariance of the results. The probability amplitudes c_f for a given state f included in the expansion are obtained after propagation of the initial state i so that the integral cross sections can be evaluated through

$$\sigma_{fi}(v) = 2\pi \int_0^\infty b\mathrm{d}b \; |c_f(b, v, t \to \infty)|^2 \tag{13}$$

for a given electronic process $i \to f$ which corresponds to either bound-bound transitions (such as electron capture) or bound-free transitions (such as ionization, taken into account through the pseudostates included in the basis sets). The details of the bound states and pseudostates used in the calculations are presented in the Appendix B.

The two collision systems under consideration are complex since composed of 3 (4) valence electrons on C^+ (C) and 2 on He so that an ab initio treatment is impossible in the present time. We therefore report results from several models using different levels of sophistication. Three models including 1 or 2 electrons have been considered for the C^+-He and C-He systems :

(i) The first is a mono-electronic model (labelled `CHe1` and `C+He1` hereafter), the only active electron, initially bound to the He center, interacting with frozen cores He^+ and C/C^+. This model can describe electron capture and target single ionization and excitation;

(ii) The second, labelled `CHe2` and `C+He2`, takes into account two electrons initially bound to He and interacting with He^{2+} and frozen core C/C^+. Compared to (i), target double excitation, double ionization and transfer-excitation can be described beyond the IPM assumption;

(iii) The third model (`C1He1` and `C+1He1`) is bielectronic and describes He as in (i), the C/C^+ projectiles binding a second electron through C^+/C^{2+} frozen cores. Projectile excitation and ionization can then be considered.

Note that these models take into account only a limited number of electrons and cannot systematically describe the spin symmetry of the atomic states : for example, considering only 1 electron shrinks the He states to doublet while He is correctly represented by a spin-adapted (singlet) wavefunction in (ii). For C-He collisions we then consider a fourth, tri-electronic, model (iv), labelled `C2He1`, to describe correctly the spin multiplicity (quartet) of the lower-lying bound state of the anion C^- ‖: 1 electron is bound to He while 2 electrons sit initially on C. Finally, in order to describe the double electron capture in $C^+ - He$ collisions, *i.e.* $C^+ + He \rightarrow C^-(^2D) + He^{2+}$ insomuch as double electron capture into the ^4S ground state of C^- is spin forbidden, we consider a fifth three-electron model (v), labelled `C+1He2`, with two electrons initially bound to He and one electron sitting on C^+.

Note that in our computations we keep the energy of the states as closed as possible from the exact values of the considered systems. We especially concentrate on the production of good quality ground states for both partners since these latters contribute dominantly in the dynamics: electron capture to the ground state indeed contributes to more than 85% of the total capture cross sections. For that purpose, the basis for each simulation, given in appendix B, are optimized to obtain the energies of the fundamental and the few first excited states as closed as possible to the tabulated values.

4. Results

In this Section, we first focus on the primary C^+,C-Ar,He ion-atom and atom-atom collisions which are the basic ingredients of the IAE simulations. Collisional results involving the C_n^+ clusters then follow.

4.1. Cross sections in primary C^+,C - Ar and He collisions

4.1.1. C^+,C-Ar collisions. We display in Table 3 the comparison between measured and calculated cross sections for processes occurring in C^+,C-Ar collisions. The theoretical data stem from CTMC one-electron probabilities presented in Appendix C.1, folded into a IPM treatment. A good agreement is observed for single ionization of C^+. However the comparison gets worse for the charge exchange processes: the calculations overestimate slightly the single capture process $C^+ + Ar \rightarrow C + Ar^+$ and a huge discrepancy between experiments and theory appears for the double electron transfer process $C^+ + Ar \rightarrow C^- + Ar^{2+}$. The failure of IPM to provide an accurate description of two (and more) electron transitions has already be noted in textbooks [23] and previous investigations (see, e.g., [43, 47]). It is generally ascribed to the static potential which is employed to describe the electron-electron interaction since this latter varies in the course of the real two-electron dynamics. For C impact, we note in Table 3 that the merging of CTMC and IPM yields a cross section for single capture in rather

‖ The C^- ion carries two bound states : the ^4S state bound by about 1.263 eV and the very loose bound (33 meV) ^2D state [46]. In our basis sets this latter lies just above threshold.

Table 3. Comparison between measured and calculated cross sections (in cm^2) for ionization and charge exchange processes in C^+,C-Ar collisions at v=2.25.

Process	Experiments (rel. error)	CTMC+IPM
$C^+ \rightarrow C^{2+}$	2.9×10^{-16} (28%)	2.9×10^{-16}
$C^+ \rightarrow C$	1.4×10^{-17} (29%)	4.1×10^{-17}
$C^+ \rightarrow C^-$	3.1×10^{-20} (33%)	2.0×10^{-18}
$C \rightarrow C^-$	5.8×10^{-18} (33%)	1.1×10^{-17}

Table 4. Comparison between measured and calculated cross sections (in cm^2) for processes occurring in C^+,C-He collisions. All results are for v=2.25 with exception of [48] (v=2) and [49] (v=2.45).; $\diamond$: double electron capture onto the ^2D excited state of C^-.

Process	Experiments (rel.error)	SCAOCC+IPM	calculation type
Projectile single ionization			
$C^+ \rightarrow C^{++}$	1.5 10^{-16} (32%)	1.3 10^{-16}	(`C+1He1`)
$C \rightarrow C^+$	1.8 10^{-16} (10%)[50]	1.1 10^{-16}	(`C1He1`)
Target single and double ionization			
$He \rightarrow He^+$ (incident C^+)	1.8 10^{-16} (20%)[48]	1.9 10^{-16}	(`C+He1`)
$He \rightarrow He^{++}$ (incident C^+)	0.3 10^{-16} (30%)[48]	0.5 10^{-16}	(`C+He1`)
$He \rightarrow He^+$ (incident C)	1.4 10^{-16} (15%)[49]	1.7 10^{-16}	(`CHe1`)
$He \rightarrow He^{++}$ (incident C)	0.14 10^{-16} (15%)[49]	0.4 10^{-16}	(`CHe1`)
Single transfer to the projectile			
$C^+ \rightarrow C$	3.5 10^{-17} (15%)	3.7 10^{-17}	(`C+1He1`)
$C \rightarrow C^-$	0.55 10^{-17} (15%)	0.36 10^{-17}	(`C2He1`)
Double transfer to the projectile			
$C^+ \rightarrow C^-$	8.0 10^{-20} (20%)	3.3 10^{-20} $\diamond$	(`C+1He2`)

good agreement with experiments. This confirms that CTMC+IPM is satisfactory for single-electron processes.

4.1.2. C^+,C-He collisions. We compare in Table 4 measured and calculated cross sections for various processes occurring in C^+,C-He collisions at v=2.25. The calculations are based on IPM, using one-electron probabilities stemming from SCAOCC computations with different levels of sophistication (specified in Table 4). These probabilities are presented in Appendix C.2, with special emphasis on the role of electronic correlations in He-induced capture processes.

Cross sections for single ionization of the projectile have been computed under the assumption that the underlying one-electron probabilities for 2s and 2p electrons are equal. For C^+-He, the calculation is in good agreement with the experimental value. The computed cross section is somewhat too low in the case of C-He collisions.

For target ionization, we compare in Table 4 the present calculations, performed

at v =2.25, with experiments performed at slightly different impact velocities, v =2 and v =2.45 in the respective cases of C^+ and C impacts. A satisfactory agreement is reached, particularly for results with incident C when taking into account the velocity dependence of ionization cross sections (see Table 8 and figure 5).

For single electron capture, including $C^+ \rightarrow C$ neutralization and $C \rightarrow C^-$ process, a good agreement is found between experimental and calculated cross sections. This indicates that the underlying one-electron capture probabilities, derived from the sophisticated `C+1He1` and `C2He1` SCAOCC models, are accurate; in other words, these models reliably describe the electronic correlations which play an important role in these charge exchange processes.

Concerning the $C^+ \rightarrow C^-$ process, we have already noted that double electron capture into the $C^-(^4S)$ ground state is spin forbidden. Accordingly, the description of double electron capture with IPM is meaningless. Therefore we report in Table 4 the three-electron calculation of type (`C+1He2`) for double electron capture into the excited $C^-(^2D)$ state. We find that this calculation provides the right order of magnitude for the double electron capture cross sections. We also have to note that contribution of double electron capture into the ^{4}S state of C^- from metastable $C^+(^4P)$ state, that would increase the experimental value, is also possible (see experimental section).

Altogether we find a satisfactory agreement between experiment and SCAOCC calculations in the basic C^+-He and C-He systems, which is a perfect condition for application of IAE to cluster-atom collisions. We now present results obtained in these systems, process by process.

4.2. Projectile ionization in C_n^+-Ar,He collisions.

We present in Table 5 and illustrate in Figs. 2(a,b) the experimental and IAE cross sections for projectile ionization in C_n^+-Ar,He collisions at v=2.25. It has to be noted that the results for the helium target are very close to those obtained in previous experiments performed at v=2.6. [22]. The agreement between measured and computed cross sections is satisfactory, especially in the case of He target. We are thus led to note that contrarily to what happened for electron capture, the IPM (inherent in the IAE approximation employed to compute the cross sections with cluster projectiles) is reasonable, not only for single but also for multiple ionization processes. This indicates that electron-electron correlations influence less the ionization processes in which electrons are ejected in the continuum than the multiple capture processes where the electrons finally lie close to each other.

We observe in Figs. 2(a,b) that the ionization cross sections monotically increase as a function of n, number of centers in the clusters. This quasi linear behaviour is quite intuitive: it reflects the fact that each neutral center within the cluster contributes to the ionization cross sections. Nevertheless the slope of the increase is changing with the target. This is due to multiple ionization. Indeed, in the helium target case where double ionization is small, the slope of single ionization with n is about 0.6 while in

Table 5. Experimental and calculated (IAE) projectile ionization cross sections (cm^2) in C_n^+-Ar,He collisions at v=2.25. Values with asterisks were obtained using the present single ionization at v =2.25 and experimental multiple to single ratios at v =2.6.

Process	Exp. (Ar target)	IAE (Ar target)	Exp. (He target)	IAE (He target)
$C^+ \rightarrow C^{2+}$	2.9×10^{-16} (28%)	2.9×10^{-16}	1.5×10^{-16} (32%)	1.3×10^{-16}
$C^+ \rightarrow C^{3+}$		1.2×10^{-16}		1.6×10^{-17}
$C_2^+ \rightarrow [C_2^{2+}]$	2.9×10^{-16} (24%)	4.0×10^{-16}	2.7×10^{-16} (15%)	2.0×10^{-16}
$C_2^+ \rightarrow [C_2^{3+}]$		2.3×10^{-16}	4.4×10^{-17} (17%)	4.3×10^{-17}
$C_3^+ \rightarrow [C_3^{2+}]$		4.5×10^{-16}	2.8×10^{-16} (11%)	2.6×10^{-16}
$C_3^+ \rightarrow [C_3^{3+}]$		2.7×10^{-16}	6.7×10^{-17} (15%)	6.9×10^{-17}
$C_4^+ \rightarrow [C_4^{2+}]$	4.0×10^{-16} (28%)	5.3×10^{-16}	4.0×10^{-16} (30%)	3.4×10^{-16}
$C_4^+ \rightarrow [C_4^{3+}]$	2.2×10^{-16} (28%)	3.4×10^{-16}	1.0×10^{-16} (30%)	9.3×10^{-17}
$C_4^+ \rightarrow [C_4^{4+}]$	1.4×10^{-16} (35%)	2.5×10^{-16}	2.6×10^{-17} (40%)*	2.2×10^{-17}
$C_4^+ \rightarrow [C_4^{5+}]$	6.8×10^{-17} (35%)	1.9×10^{-16}	5.6×10^{-18} (40%)*	4.3×10^{-18}
$C_5^+ \rightarrow [C_5^{2+}]$		5.8×10^{-16}	5.0×10^{-16} (15%)	4.0×10^{-16}
$C_5^+ \rightarrow [C_5^{3+}]$		3.8×10^{-16}	1.6×10^{-16} (17%)	1.2×10^{-16}

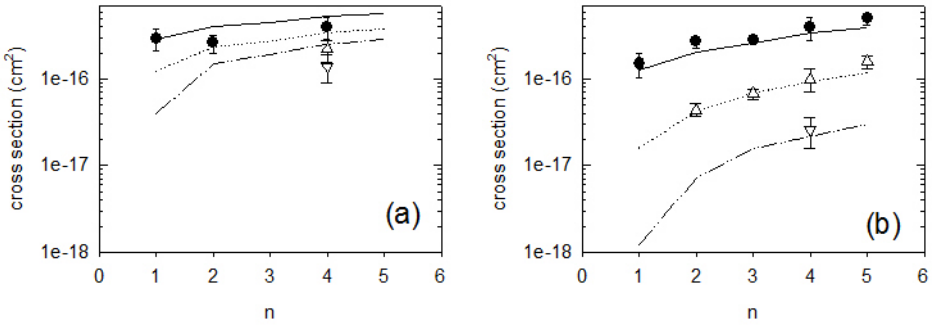

Figure 2. Comparison between measured and calculated projectile ionization cross sections (cm^2) in C_n^+-Ar (a) and C_n^+-He (b) collisions at v=2.25. Experiments: single ionization (circles), double ionization (triangles up), triple ionization (triangles down). IAE results: single ionization (solid lines), double ionization (dotted lines), triple ionization (dash-dot-dot lines).

the argon case, for which multiple ionization processes are much larger, the increase is weaker, with a slope of 0.2. Globally IAE reproduces satisfactorily these dependences, which shows that the atomic approach inherent in this model makes sense.

Coming back to the atomic case ($n = 1$) the single ionization cross section is two times larger for Ar impact than for He impact (see Table 5). The comparison of Ar- and He-induced one-electron probabilities for C^+ ionization, respectively displayed in Fig. C1 and Fig. C3(a) of Appendix C, allows us to understand this: these probabilities cover the same range of impact parameters (typically $b \leq 3$) but the Ar-induced probability is significantly larger than its He counterpart. From a physical point of view, as C^+ crosses

Table 6. Experimental and calculated (IAE) neutralization cross sections (cm^2) in C_n^+-Ar,He collisions at v=2.25.

Process	Exp.(Ar)	Calc.(Ar)	Exp.(He)	Calc.(He)
$C^+ \rightarrow C$	1.4 10^{-17} (30%)	4.1 10^{-17}	3.5 10^{-17} (15%)	3.7 10^{-17}
$C_2^+ \rightarrow [C_2]$	2.2 10^{-17} (25%)	3.0 10^{-17}	3.9 10^{-17} (15%)	3.5 10^{-17}
$C_3^+ \rightarrow [C_3]$		2. 10^{-17}	4.2 10^{-17} (10%)	3.2 10^{-17}
$C_4^+ \rightarrow [C_4]$	1.5 10^{-17} (27%)	2.6 10^{-17}	3.9 10^{-17} (15%)	3.4 10^{-17}
$C_5^+ \rightarrow [C_5]$		2.6 10^{-17}	5.3 10^{-17} (15%)	3.6 10^{-17}

preferentially the He and Ar targets at the same $b \approx 2$, it sees a He nuclear charge almost completely screened by its two orbiting electrons (leading to a total effective charge $Z_{eff} \approx 0$) while it enters into the (more diffuse) Ar electron density so that the screening is not complete in this case ($Z_{eff} \neq 0$). It can be easily understood that ionization is enhanced in the latter case so that the Ar-induced single ionization cross section is larger than the He-induced one. This argument also applies to C impact. That is the reason why the computed cross sections for single ionization of C_n^+ clusters are always larger when they are induced by Ar (see Table 5). Experimentally the effect is not as clear (with exception of n=1) but experimental results are in fact compatible with the theoretical trend when taking into account the error bars.

For multi-ionization both calculated and measured cross sections exhibit a strong target dependence. Multi-ionization cross sections are much larger with Ar than with He, an effect that increases with the ionization degree. This result has two origins. The first one relates to the screening effect discussed above in ion(atom)-atom collisions. As well known in ion-atom collisions, IPM probabilities associated to multi-ionization processes strongly peak at small impact parameters (typically $b \lesssim 1$), and this shrinking effect towards small b is larger the higher is the ionization multiplicity. From a computational point of view, the shrinking comes from the p_{ion}^m factor entering the probability associated to m-fold ionization, where p_{ion} is the one-electron probability. Intuitively we understand that multiple ionization requires 'hard' (*i*.e. small b) collisions. As b decreases, the projectile deeply penetrates into the target core where the screening of the nuclear charge progressively vanishes. Accordingly, $Z_{eff}(\mathrm{Ar}) >> Z_{eff}(\mathrm{He})$, which results in larger cross sections for Ar-induced multiple ionization. For instance, calculated double over single ionisation cross sections ratios DI/SI are equal to 13% for He and to 43% for Ar (see Table 5, n=1 results). In addition the effect is reinforced in clusters due to the ionization of different centers that also involves product of probabilities. This multicenter effect is clearly visible, responsible of the increase of DI/SI with the cluster size. For instance, for He, this calculated ratio increases from 13% (n=1) to 30% (n=5) whereas for Ar this increase is from 43% (n=1) to 65% (n=5).

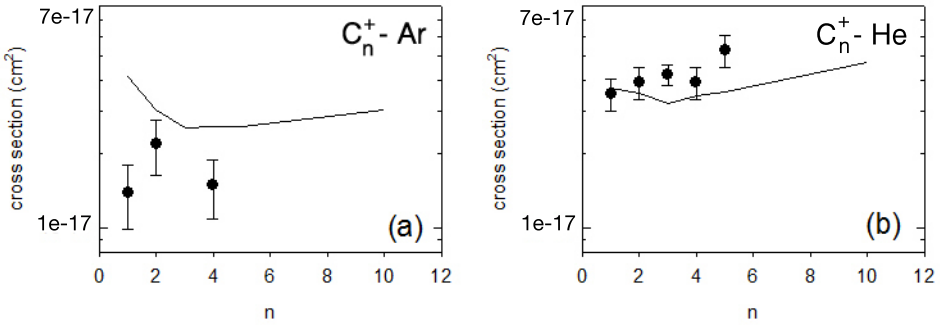

Figure 3. Comparison between measured and calculated projectile neutralization cross sections (cm^2) in C_n^+-Ar (a) and C_n^+-He (b) collisions at v=2.25. Experiment: circles; IAE calculations: solid lines.

4.3. Neutralization in C_n^+-Ar,He

In Table 6 and Figures 3(a,b) we present experimental and calculated neutralization cross sections in C_n^+-Ar,He collisions. Despite the few experimental points, measurements with the argon target are found compatible with those involving helium, namely constant values of the cross section at small cluster sizes, followed by a slight increase at large sizes. This increase is due to electron capture onto neutral C constituents, the weight of which increases with n. Indeed, neglecting this process (*i.e.* considering electron capture onto the C^+ ion only) leads to neutralization cross sections decreasing with increasing cluster size, in contradiction with the experimental trends; in the helium case for instance, the neutralization cross section for n=10 would be reduced by 30% compared to n=1. The role of the electron capture onto neutral constituents in the cluster size dependence of neutralization cross sections, put forward in [20], is here confirmed. On the other hand, the cross section increase is counterbalanced by projectile ionization which is responsible of the decrease of neutralization cross sections predicted by IAE calculations at small cluster sizes (n=1-3). This decrease is particularly strong for the argon target case since projectile ionization is larger (see Fig. C1 and Fig. C3(a) of Appendix C). The influence of this process can also be seen indirectly by comparing the absolute values of neutralization cross sections with helium and argon. Indeed, if we neglect projectile ionization in IAE, we find neutralization cross sections larger with argon than with helium (four times larger for n=4 for instance), at variance with experiment. Altogether, a comprehensive interpretation of the experimental results is furnished by the theory.

4.4. Anionic production in C_n^+-Ar,He

In Table 7 and Figure 4(a,b) we present experimental and calculated anionic production cross sections $C_n^+ \rightarrow [C_n^-]$ in C_n^+-Ar,He collisions. Experimentally we observe larger cross sections in the helium target case as compared to argon, which is due to the fact

Table 7. Experimental and calculated (IAE) anionic production cross sections (cm^2) in C_n^+-Ar,He collisions at v=2.25.

Process	Exp.(Ar)	Calc.(Ar)	Exp.(He)	Calc.(He)
$C^+ \rightarrow C^-$	3.1 10^{-20} (50%)	2.0 10^{-18}	8.0 10^{-20} (20%)	6.8 10^{-20}
$C_2^+ \rightarrow [C_2^-]$	1.8 10^{-20} (36%)	1.2 10^{-18}	3.4 10^{-20} (36%)	1.0 10^{-19}
$C_3^+ \rightarrow [C_3^-]$		8.6 10^{-19}	1.6 10^{-20} (22%)	1.6 10^{-19}
$C_4^+ \rightarrow [C_4^-]$	2.7 10^{-21} (52%)	8.1 10^{-19}	1.0 10^{-20} (40%)	1.6 10^{-19}
$C_5^+ \rightarrow [C_5^-]$		7.3 10^{-19}	2.0 10^{-20} (30%)	1.8 10^{-19}

that projectile ionization is larger with argon than with helium. The experimental size evolution of the cross sections is similar in the two cases. By contrast, IAE predictions differ significantly with the two targets. This is due to the treatment of double electron capture onto the C^+ ion. In the argon case, an independent electron treatment has been performed and this contribution, which is very large (see n=1), dominates for all sizes. Only a small decrease, associated to projectile ionization, is observed. In the helium-target case a calculation, taking into account the electron correlations, has been performed. The associated value, in much better agreement with the experiment (n=1), is small as compared to the contribution due to electron capture onto different centers. This last contribution is responsible for the increase of the cross section between n=1 and n=3 whereas a saturation is finally reached $n > 3$. With helium as with argon, we see that the experimental size evolution is not reproduced at all by the calculation. We suspect, as discussed in [20], the electron loss of the loosely bound electron to be at the origin of the experimental decrease. Indeed, $[C_n^-]$ species are produced in excited states as it can be inferred from the large measured dissociation branching ratios (see experimental section). These excited states are amenable to relaxation through electron emission, and the effect increases with increasing cluster size at large internal energies [20]. This issue deserves to be further investigated. Unfortunately, the separation of target and projectile electron emissions is very difficult to make at the impact velocities considered herein [51].

4.5. Target ionization in C_n^+-He

In Table 8 are reported single and double ionization cross sections of helium in C^+,C_4^++He collisions at v=2, 2.6 and 4 (experiment) and v=2.25 (IAE calculation). We presented in section 4.1.2 the case of the C^+-He collision and noted that the agreement between experiment and calculation was rather satisfactory. Results in Table 8 and Figure 5 report on the first application of IAE to target ionization induced by cluster projectiles. We find that the large experimental increase of the cross sections with incident C_4^+ as compared to C^+, is pretty well reproduced by the IAE calculations. This effect is due to the fact that somehow four collisions operate with C_4^+ as compared to C^+. Still the agreement was not guaranteed considering the fact that IAE is performing

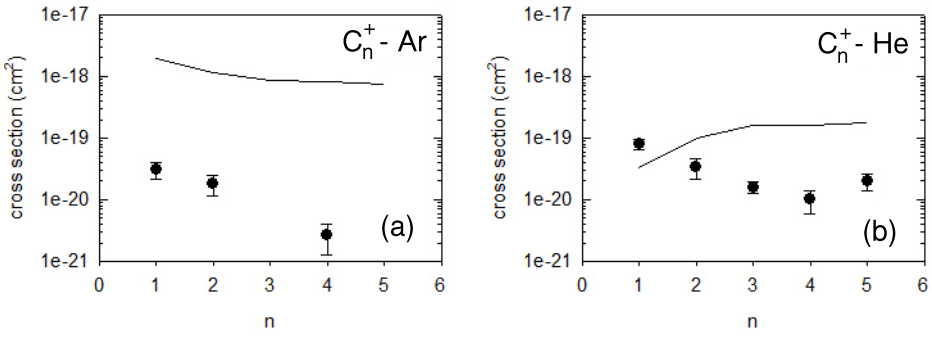

Figure 4. Comparison between measured and calculated anionic production cross sections $C_n^+ \rightarrow [C_n^-]$ (cm^2) in C_n^+-Ar (a) and C_n^+-He (b) collisions at v=2.25. Experiment: circles; IAE calculations: solid lines.

Table 8. Experimental (v=2, 2.6, 4) and calculated (v=2.25) ionization cross sections of helium (cm^2) (rel.error in %) in C^+,C_4^+-He collisions.SI and DI refer to pure single and double ionization of helium respectively

Velocity	HE SI, inc.C^+	HE DI, inc.C^+	HE SI, inc.C_4^+	HE DI, inc.C_4^+
2	1.8 10^{-16} (20%)	3.1 10^{-17} (26%)	7.3 10^{-16} (16%)	1.6 10^{-16} (18%)
2.25	1.9 10^{-16}	5.1 10^{-17}	5.1 10^{-16}	2.0 10^{-16}
2.6			4.2 10^{-16} (22%)	1.3 10^{-16} (29%)
4	7.0 10^{-17} (35%)	1.2 10^{-17} (45%)	3.2 10^{-16} (26%)	7.8 10^{-17} (29%)

a sum of probabilities whereas a sum of amplitudes, for a given final state, should be considered instead. Indeed, within the approximate representation of the cluster into independent atoms, the ionization of different atoms corresponds to different final states but this is not true for target ionization. This proves that interference terms are small (or cancel) and this extends the applicability of the IAE model, so far tested on projectile ionization and electron capture, to target ionization as well.

5. Conclusions

We have presented a joint experimental and theoretical study of single and multiple electron capture and ionization processes in high velocity $C_{n\leq 5}^+$-He,Ar collisions. Experimentally the method required the coincident detection and identification of all projectile fragments, eventually in coincidence with recoil ions (for the He-target ionization). In order to check the reliability of probabilities used in the theoretical modelling we also measured the electron capture cross sections in C-He,Ar collisions. This was done by performing a target thickness dependence of C^- production cross sections. From the theoretical side we modelled the electronic processes within the IAE (Independent Atom and Electron) approximation relying on probabilities from ion-atom and atom-atom collision calculations. We used state-of-the-art calculations to

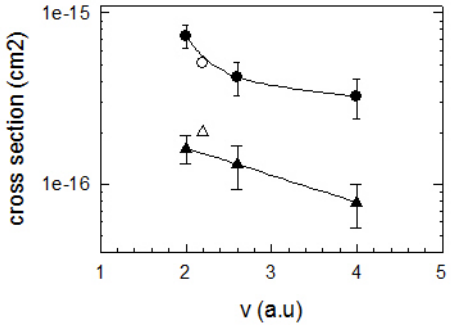

Figure 5. Single (circles) and double (triangles) target ionization cross sections (cm^2) in C_4^+-He collisions as a function of the projectile velocity v. Black symbols: Experiments at v=2,2.6,4.; open symbols: IAE calculation at v=2.25. Lines are to guide the eye.

obtain these probabilities, namely, CTMC and SCAOCC calculations for Ar and He targets respectively. In this last case various calculations, taking into account up to three active electrons, were performed in order to test the accuracy of the independent electron approximation.

We found a general good agreement between measured and IAE cross sections. For projectile ionization, IAE predictions are in very good agreement with experiment in the C_n^+-He collisions whereas it predicted right orders of magnitude for the cross sections in the C_n^+-Ar systems, in particular the large multiple ionization cross sections. For neutralization of C_n^+ the agreement is better in the helium target case than in the argon target case but it has to be noted that in this last case we start already with a discrepancy for n=1. Still, due to the role of projectile ionization, IAE predicts cross sections smaller with argon than with helium in perfect agreement with experiment. Finally, for He target ionization in C_n^+-He collisions, the agreement is satisfactory . This allows to extend the applicability of the IAE model, previously tested on projectile ionization and electron capture, to this process as well.

In contrast with the above discussed processes, the anionic production cross sections are not well predicted by IAE. In the argon target case the discrepancy is already huge for the n=1 which proves that double electron capture cannot be treated on the basis of independent electrons. This is illustrated for the helium target case where comparison between experiment and SCAOCC calculations including electron correlations shows a tremendous improvement. In both cases though, the size evolution of cross sections differ between experiments and IAE predictions. We suspected the loss of loosely bound electrons to be at the origin of the discrepancy. Indeed, for the anions, electron emission is a probable relaxation channel, which deserves further investigation.

Acknowledgments

People having worked in AGAT collaboration over the years are indebted for their valuable help in measurements. This work has been partially supported by the project ENE2011-28200 of the Secretaria de Estado de Investigacion, Desarrollo e Innovacion (Spain). We acknowledge computational facilities provided by the Mésocentre de Calcul Intensif Aquitain at University of Bordeaux [52] and the Centro de Computacion Cientifica at Universidad Autonoma de Madrid. Part of this work (GL and AD) was supported by French state funds managed by the ANR within the Investissements d'Avenir programme under reference ANR-11-IDEX-0004-02.

References

[1] Brechignac C, Cahuzac P, Concina B, Leygnier J and Tigneres I 2000 *European Physical Journal D* **12** 185

[2] Fayeton J, Barat M, Brenot J, Dunet H, Picard Y, Saalmann U and Schmidt R 1998 *Physical Review A* **57** 1058

[3] Bergen T, Brenac A, Chandezon F, Guet C, Lebius H, Pesnelle A and Huber B 2001 *European Physical Journal D* **14** 317

[4] Campbell E and Rohmund F 2000 *Reports on Progress in Physics* **63** 1061

[5] Wohrer K, Chabot M, Rozet J, Gardes D, Vernhet D, Jacquet D, DellaNegra S, Brunelle A, Nectoux M, Pautrat M, LeBeyec Y, Attal P and Maynard G 1996 *Journal of Physics B-Atomic Molecular and Optical Physics* **29** L755

[6] Ouaskit S, Farizon B, Farizon M, Gaillard M, Chevarier A, Chevarier N, Gerlic E and Stern M 1994 *International Journal of Mass Spectroscopy and Ion Processes* **139** 141

[7] Tappe W, Flesch R, Ruhl E, Hoekstra R and Schlatholter T 2002 *Physical Review Letters* **88** 143401

[8] Zettergren H, Schmidt H T, Reinhed P, Cederquist H, Jensen J, Hvelplund P, Tomita S, Manil B, Rangama J and Huber B A 2007 *Journal of Chemical Physics* **126** 224303

[9] de Vries J, Hoekstra R, Morgenstern R and Schlatholter T 2002 *Journal of Physics B-Atomic Molecular and Optical Physics* **35** 4373

[10] Hvelplund P, Liu B, Nielsen S and Tomita S 2003 *International Journal of Mass Spectroscopy* **225** 83

[11] Postma J, Bari S, Hoekstra R, Tielens A G G M and Schlathoelter T 2010 *Astrophysical Journal* **708** 435

[12] Holm A I S, Zettergren H, Johansson H A B, Seitz F, Rosen S, Schmidt H T, Lawicki A, Rangama J, Rousseau P, Capron M, Maisonny R, Adoui L, Mery A, Manil B, Huber B A and Cederquist H 2010 *Physical Review Letters* **105** 213401

[13] Brechignac C, Cahuzac P, Concina B, Leygnier J, Ruiz L, Zarour B, Hervieux P, Hanssen J, Politis M and Martin F 2002 *Physical Review Letters* **89** 183402

[14] Rentenier A, Ruiz L F, Diaz-Tendero S, Zarour B, Moretto-Capelle P, Bordenave-Montesquieu D, Bordenave-Montesquieu A, Hervieux P A, Alcami M, Politis M F, Hanssen J and Martin F 2008 *Physical Review Letters* **100** 183401

[15] Galassi M, Rivarola R and Fainstein P 2004 *Physical Review A* **70** 032721

[16] Illescas C, Errea L F, Mendez L, Pons B, Rabadan I and Riera A 2011 *Physical Review A* **83** 052704

[17] Murakami M, Kirchner T, Horbatsch M and Luedde H J 2012 *Physical Review A* **85** 052704

[18] Murakami M, Kirchner T, Horbatsch M and Luedde H J 2012 *Physical Review A* **86** 022719

[19] Agnihotri A N, Kasthurirangan S, Nandi S, Kumar A, Galassi M E, Rivarola R D, Fojon O, Champion C, Hanssen J, Lekadir H, Weck P F and Tribedi L C 2012 *Physical Review A* **85** 032711

[20] Beroff K, Chabot M, Martinet G, Pino T, Bouneau S, Le Padellec A, Feraud G, Do Thi N, Calvo F, Bordas C and Lepine F 2013 *Journal of Physics B-Atomic Molecular and Optical Physics* **46** 015201

[21] Wohrer K and Watson R 1993 *Physical Review A* **48** 4784

[22] Mezdari F, Wohrer-Beroff K, Chabot M, Martinet G, Della Negra S, Desesquelles P, Hamrita H and Le Padellec A 2005 *Physical Review A* **72** 032707

[23] Bransden B and McDowell M 1992 *Charge exchange and the theory of Ion-Atom collisions* (Oxford: Clarendon Press)

[24] Olson R E and Salop A 1977 *Physical Review A* **16** 531–541

[25] Illescas C and Riera A 1999 *Physical Review A* **60** 4546

[26] Olson R E 1979 *Journal of Physics B Atomic Molecular Physics* **12** L109–L113

[27] Dimitriou K, Katsonis K and Maynard G 2000 *Journal de Physique IV (France)* **10** 299 International Conference on Strongly Coupled Coulomb Systems, ST MALO, FRANCE, SEP 04-10, 1999
[28] Fritsch W and Lin C 1991 *Physics Reports* **202** 1
[29] Toshima N 1999 *Physical Review A* **59** 1981
[30] Wohrer K, Fosse R, Chabot M, Gardes D and Champion C 2000 *Journal of Physics B-Atomic Molecular and Optical Physics* **33** 4469
[31] Luna H, Zappa F, Martins M, Magalhaes S, Jalbert G, Coelho L and Faria N 2001 *Physical Review A* **63** 052716
[32] Chabot M, Martinet G, Mezdari F, Diaz-Tendero S, Beroff-Wohrer K, Desesquelles P, Della-Negra S, Hamrita H, Le Padellec A, Tuna T, Montagnon L, Barat M, Simon M and Ismail I 2006 *Journal of Physics B-Atomic Molecular and Optical Physics* **39** 2593
[33] Tuna T 2008 Phd thesis, paris sud university, unpublished
[34] Martinet G, Diaz-Tendero S, Chabot M, Wohrer K, Della Negra S, Mezdari F, Hamrita H, Desesquelles P, Le Padellec A, Gardes D, Lavergne L, Lalu G, Grave X, Clavelin J, Hervieux P, Alcami M and Martin F 2004 *Physical Review Letters* **93** 063401
[35] McGuire J H and Weaver L 1977 *Physical Review A* **16** 41–47
[36] Lüdde H and Dreizler R 1985 *Journal of Physics B-Atomic Molecular and Optical Physics* **18** 107
[37] Monti J M, Fojon O A, Hanssen J and Rivarola R D 2013 *Journal of Physics B-Atomic Molecular and Optical Physics* **46** 145201
[38] Abrines R and Percival I C 1966 *Proceedings of the Physical Society* **88** 861–872
[39] Reinhold C and Falcon C 1986 *Physical Review A* **33** 3859
[40] Eichenauer D, Grun N and Scheid W 1981 *Journal of Physics B Atomic Molecular Physics* **14** 3929–3941
[41] Hardie D and Olson R 1983 *Journal of Physics B-Atomic Molecular and Optical Physics* **16** 1983
[42] Rakovic M, Schultz D, Stancil P and Janev R 2001 *Journal of Physics A-Mathematical and General* **34** 4753
[43] Guzman F, Errea L F and Pons B 2009 *Physical Review A* **80** 042708
[44] Caillat J, Dubois A, Sundvor I and Hansen J 2004 *Physical Review A* **70** 032715
[45] Sisourat N, Pilskog I and Dubois A 2011 *Physical Review A* **84** 052722
[46] Andersen T 2004 *Physics Reports* **394** 157–313
[47] Errea L, Gorfinkiel J, Harel C, Jouin H, Macias A, Mendez L, Pons B and Riera A 2000 *Journal of Physics B-Atomic Molecular and Optical Physics* **33** 3107
[48] Beroff K et al 2014 Unpublished
[49] DuBois R and Toburen L 1988 *Physical Review A* **38** 3960–3968 ISSN 1050-2947
[50] Nakai Y and Sataka M 1991 *Journal of Physics B-Atomic Molecular and Optical Physics* **24** L89
[51] Toburen L, DuBois R, Reinhold C, Schultz D and Olson R 1990 *Physical Review A* **42** 5338
[52] http://www.mcia.univ-bordeaux.fr
[53] Leredde A, Cassimi A, Flechard X, Hennecart D, Jouin H and Pons B 2012 *Physical Review A* **85** 032710
[54] http://www.physics.nist.gov
[55] Pons B 2000 *Physical Review Letters* **84** 4569
[56] Pons B 2001 *Physical Review A* **63** 012704
[57] Muller H 1999 *Physical Review A* **60** 1341
[58] Schmidt M, Balridge K, Boatz J, Elbert S, Gordon M, Jensen J, Koseki S, Matsunaga N, Nguyen K, Su S, Windus T, Dupuis M and Montgomery J 1993 *Journal of Computational Chemistry* **14** 1347
[59] Fosse R 2000 Phd thesis, paris 6 university, unpublished

	b_1	b_2	b_3
$Ar^+ + e$	5.4	1	3.682
$C + e$	1.964	7.136	0.840
$C^+ + e$	1.904	0.808	2.518
$C^{2+} + e$	2.044	1.256	3.202

Table A1. Parameters $\{b_1, b_2, b_3\}$ of the model potentials of eq. (A.1) for the $(Ar^+ + e)$, $(C + e)$, $(C^+ + e)$ and $(C^{2+} + e)$ systems

Appendix A. Model potentials

We detail herein the model potentials $V_{mod}^{(A^{q+}+e)}$ which have been employed to describe the interaction of a valence electron e with a frozen ionic ($q > 0$) or atomic ($q = 0$) core. For $A \equiv Ar, C$ and $q = 0 - 2$ (see eqs. (8)-(11)), $V_{mod}^{(A^{q+}+e)}$ is of the form

$$V_{mod}^{(A^{q+}+e)}(r) = -\frac{Z-N}{r} - \frac{b_1 \exp(-b_2 r) + (N-A)\exp(-b_3 r)}{r} \qquad \text{(A.1)}$$

where r is the electron-nucleus radial distance, Z is the nuclear charge and N is the number of frozen electrons so that $q = Z - N$. $\{b_1, b_2, b_3\}$ are parameters which are optimized to reproduce as accurately as possible the valence state energies of the $(A^{q+}+e)$ system. As detailed in [53], the optimization consists in varying the parameters $\{b_i\}$ until diagonalization of the one-electron Hamiltonian $H = -\frac{1}{2}\nabla^2 + V_{mod}^{(A^{q+}+e)}$ yields eigenenergies that match reference data. In our case, the energies of reference are those tabulated in the NIST Atomic Spectra Database [54], and H is diagonalized in large-scale (effectively complete) "even-tempered" Slater-type-orbital (STO) sets [53, 55, 56].

For the $(Ar^+ + e)$ system, we have employed the parameters $\{b_i\}$ proposed by Muller [57], which are reported in Table A1 together with those associated to the $(C^{2+} + e)$, $(C^+ + e)$ and $(C + e)$ systems. In Table A2, we compared the eigenenergies issued from the Hamiltonian diagonalizations with the reference data taken from NIST, putting special emphasis on the first excited levels which are the most difficult to represent because of the (most) significant overlap of their electron densities with that of the core. One can note a good agreement between our values and the reference ones, the largest relative difference between them not exceeding 2%.

Beyond eigenenergies, we have also checked the accuracy of our computed eigenfunctions by comparing their electron radial densities to their Hartree-Fock (HF) counterparts obtained by means of the quantum chemistry package GAMESS [58] using a triple-zeta underlying gaussian basis (called aug-cc-pVTZ). The comparison of V_{mod} and HF radial densities is presented in Fig. A1 for the fundamental $Ar(3p)$, $C(2p)$, $C^+(2p)$ and $C^-(2p)$ states. Agreement is found satisfactory.

Besides CTMC calculations, all these V_{mod} descriptions have also been employed in the SCAOCC computations. However the model potentials A.1 have then been fitted by a six Gaussian-type function in order to use standard matrix element evaluation schemes [45] in the dynamical calculations. Concerning the helium atom, whenever

$(Ar^+ + e)$		
(n,l) level	V_{mod}	NIST
4s	-0.1542	-0.1548
5s	-0.0621	-0.0621
3p	**-0.5814**	**-0.5791**
4p	-0.0971	-0.0979
3d	-0.0634	-0.0641
4d	-0.0356	-0.0356
$(C + e)$		
(n,l) level	V_{mod}	NIST
2p	**-0.0463**	**-0.0464**
$(C^+ + e)$		
(n,l) level	V_{mod}	NIST
3s	-0.1386	-0.1389
4s	-0.0591	-0.0580
2p	**-0.4138**	**-0.4139**
3p	-0.0951	-0.0933
3d	-0.0557	-0.0564
4d	-0.0313	-0.0319
$(C^{2+} + e)$		
(n,l) level	V_{mod}	NIST
3s	-0.3630	-0.3651
4s	-0.1772	-0.1797
2p	**-0.8963**	**-0.8961**
3p	-0.2980	-0.2959
3d	-0.2336	-0.2329
4d	-0.1303	-0.1301

Table A2. $(Ar^+ + e)$, $(C + e)$, $(C^+ + e)$ and $(C^{2+} + e)$ valence electron binding energies obtained from model potentiel (V_{mod}) calculations, compared to reference data taken from NIST (statiscally averaged over all possible J values). The states indicated in bold correspond to the fundamental state of each system.

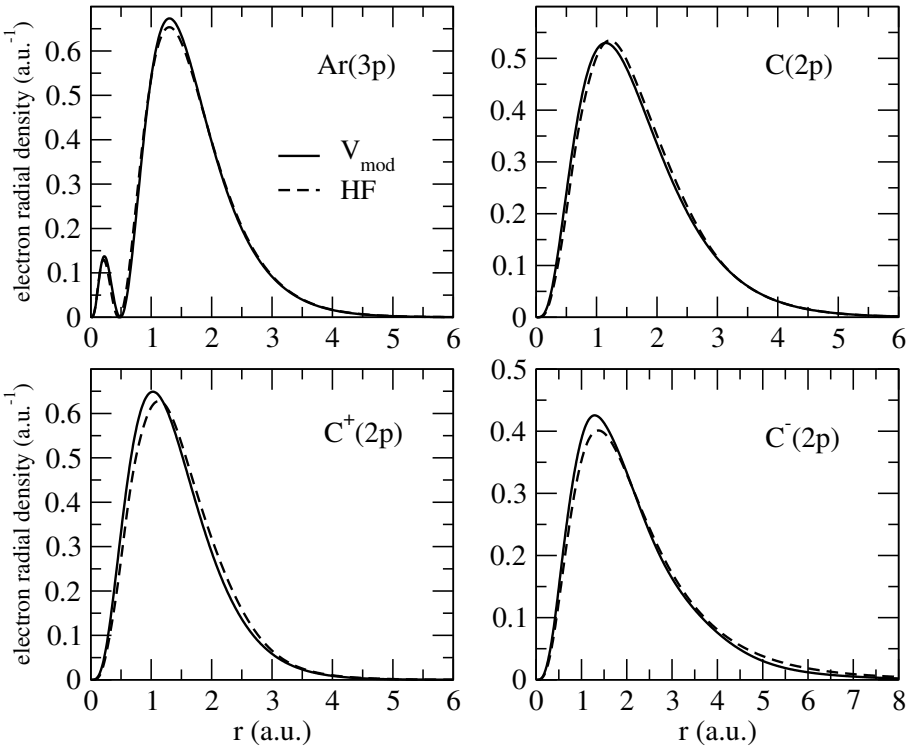

Figure A1. Comparison of electron radial densities for Ar(3p), C(2p), C^+(2p) and C^-(2p) obtained by means of the present model potentiel (V_{mod}, continuous lines) and reference Hartree-Fock (HF, dashed lines) calculations.

modelled with (only) one active electron, a model potentiel of the form

$$V_{mod}^{(He^+ + e)} = -\frac{1}{r}(1 + \exp(-\beta r^2)) \ . \tag{A.2}$$

has been used, with $\beta = 4.9262$ in order to yield the correct values (within 1%) of the binding energies of the ground state and of some excited states of He.

Appendix B. Basis sets for SCAOCC calculations

The diagonalisation of the hamiltonians related to He^+, He, C^+, C and C^- species on a set of GTOs and products of GTOs creates the states that we include in the dynamical calculations. The tables B1 and B2 summarize the different basis sets used in the calculations presented in this paper.

Appendix C. One-electron probabilities underlying the IAE calculations

For sake of completeness, we present in this section the one-electron probabilities which have been used to perform the IPM and IAE calculations of cross sections in C_n^+, C - Ar and He collisions. Special emphasis is put on the role of electronic correlations in collisions involving the He target.

Table B1. Description of the basis sets used in the three models implemented to describe C^+ - He collisions. A cell gives the number of states of specific energy and symmetry included on a center : e.g. the description of He target in model (i) includes 6 $\ell = 0$ and 4 $\ell = 1$ (total : $6 + 4 \times 3 = 18$) bound states as well as 2 $\ell = 0$ and 1 $\ell = 1$ (total : $2 + 1 \times 5$) pseudostates of positive energy. For the sake of clarity we use lowercase (uppercase) letters to name the states in monoelectronic (multielectronic) models.

Target center

	(i) `C+He1`	(ii) `C+He2`	(iii) `C+1He1`
He	$E < 0 : 6s + 4p$ $E > 0 : 2s + 1p$	$E < E\,[\mathrm{He}^+(1s)] : 3\,^1S + 2\,^1P$ $0 > E > E\,[\mathrm{He}^+(1s)] : 14\,^1S + 16\,^1P + 9\,^1D$ $E > 0 : 3\,^1S + 2\,^1P + 1\,^1D$	$E < 0 : 6s + 4p$ $E > 0 : 1s + 1p$
He^+		$E < 0 : 4s + 3p$ $E > 0 : 1p$	

Projectile center

	(i) `C+He1`	(ii) `C+He2`	(iii) `C+1He1`
C	$E < 0 : 3s + 2p$ $E > 0 : 1s + 3p$	$E < 0 : 3s + 2p$ $E > 0 : 3p$	$E < E\,[\mathrm{C}^+(2p)] : 3\,^3S + 4\,^3P + 1\,^3D$ $0 > E > E\,[\mathrm{C}^+(2p)] : 3\,^3S + 9\,^3P + 2\,^3D$ $E > 0 : 1\,^3P$
C^+			$E < 0 : 2s + 3p$ $E > 0 : 1p$

Table B2. Description of the basis sets used in the models (i) to (iii) implemented to describe C - He collisions. Notations as in Table B1

Target center

	(i) `CHe1`	(ii) `CHe2`	(iii) `C1He1`
He	$E < 0 : 6s + 4p$ $E > 0 : 2s + 1p$	$E < E\,[\mathrm{He}^+(1s)] : 3\,^1S + 2\,^1P$ $0 > E > E\,[\mathrm{He}^+(1s)] : 14\,^1S + 16\,^1P + 9\,^1D$ $E > 0 : 3\,^1S + 2\,^1P + 1\,^1D$	$E < 0 : 6s + 4p$ $E > 0 : 1s + 1p$
He^+		$E < 0 : 4s + 3p$ $E > 0 : 1p$	

Projectile center

	(i) `CHe1`	(ii) `CHe2`	(iii) `C1He1`
C^-	$E < 0 : 1p$ $E > 0 : 2p$	$E < 0 : 1p$ $E < 0 : 3p$	$E < E\,[\mathrm{C}(2p)] : 1\,^3P$ $0 > E > E\,[\mathrm{C}(2p)] : 3\,^3S + 8\,^3P + 1\,^3D$ $E > 0 : 4\,^3S + 7\,^3P + 2\,^3D$
C			$E < 0 : 2s + 2p$ $E > 0 : 2s + 1p$

Table B3. Description of the basis sets used in the model (iv) implemented to describe C - He collisions. Notations as in Table B1

	(iv) `C2He1`
He	$E<0$: $6s+4p$ $E>0$: $1s+1p$
C^-	$E<E\,[C(2p)]$: $1\,^4P$ $E\,[C^+(2p)]>E>E\,[C(2p)]$: $4\,^4S+8\,^4P+5\,^4D$ $E>E\,[C^+(2p)]$: $10\,^4S+18\,^4P+10\,^4D$
C	$E<E\,[C^+(2p)]$: $2\,^1S+4\,^1P+2\,^1D+2\,^3S+4\,^3P+1\,^3D$ $0>E>E\,[C^+(2p)]$: $8\,^1S+8\,^1P+4\,^1D+4\,^3S+10\,^3P+2\,^3D$ $E>0$: $2\,^1S+2\,^1P+2\,^1D+1\,^3S+3\,^3P+2\,^3D$
C^+	$E<0$: $3s+3p$ $E>0$: $1p$

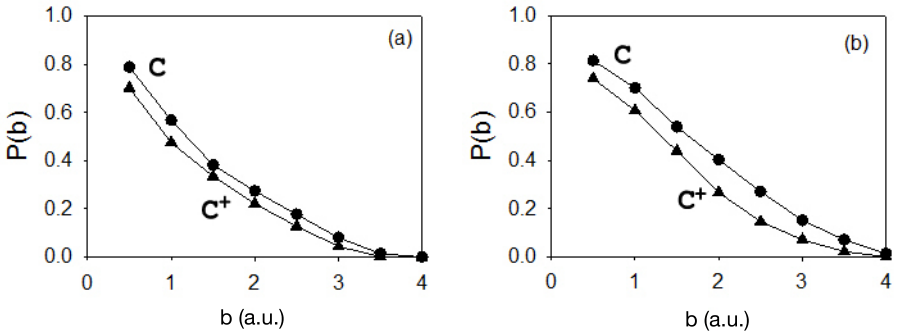

Figure C1. One-electron CTMC probabilities for $2s$ (a) and $2p$ (b) ionization of the projectile in C-Ar (circles) and C^+-Ar (triangles) collisions at v=2.25.

Appendix C.1. Primary C^+, C - Ar collisions

We display in Figures C1(a,b) the one-electron probabilities for ionization of $2s$ (Fig. C1(a)) and $2p$ (Fig. C1(b)) electrons in $C^+(2s/2p)$-Ar and $C(2s/2p)$-Ar collisions. These probabilities are obtained by means of the two-active-electron CTMC approach detailed in Section 3.2. In both collisional systems, the probability of ionizing a $2p$ electron is larger than its $2s$ counterpart. We also observe that for a given subshell, the ionization probability is larger in C-Ar than in C^+-Ar collisions.

We display in Fig. C2(a) the one-electron probabilities for target (Ar) ionization in C^+,C-Ar($3p$) collisions. These probabilities are issued from the one-active-electron CTMC approach (see Section 3.2). Ionization is found to be slightly larger in the case of C^+ impinging projectiles than in the corresponding C case: even at such high velocity this is expected since positively charged projectiles pull out target electrons more efficiently than neutral atoms. This behaviour is more conspicuous for charge exchange: as shown in Fig. C2(b), the probability for electron capture onto C^+ in C^+-

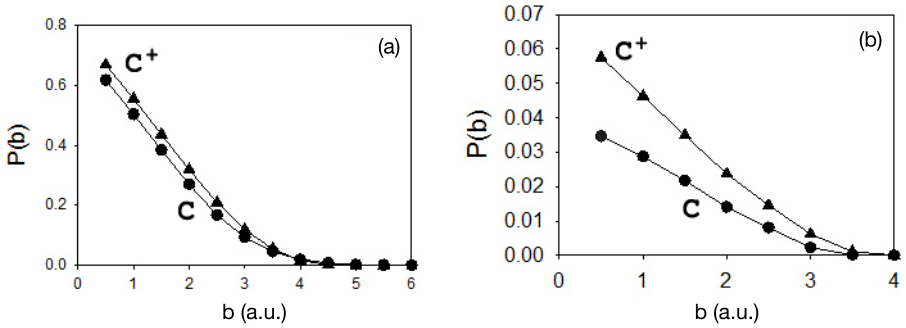

Figure C2. (a): One-electron CTMC probabilities for C + Ar → C + Ar^+ + e (circles) and C^+ + Ar → C^+ + Ar^+ + e (triangles) ionization processes at v=2.25 ; (b): One-electron CTMC probabilities for C + Ar → C^- + Ar^+ (circles) and C^+ + Ar → C + Ar^+ (triangles) charge exchange processes at v =2.25.

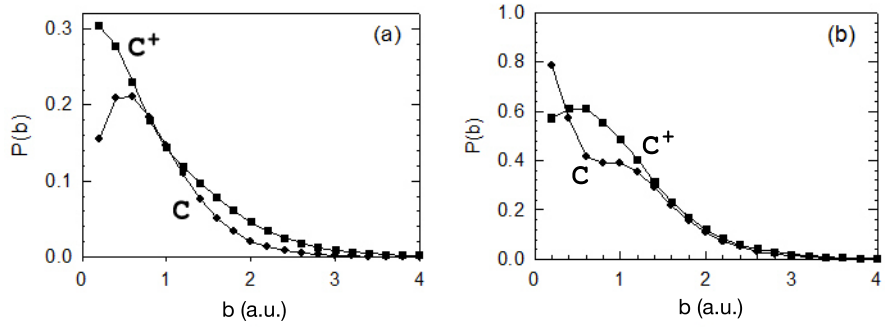

Figure C3. (a): One-electron SCAOCC probabilities for 2p projectile ionization in C (circles) and C^+ (squares) - He collisions at v=2.25; (b): same legend as (a) for 1s He-target ionization.

Ar collisions is significantly larger than the corresponding one in C-Ar collisions. It is worth noting that the two processes operate in the same impact parameter domain.

Appendix C.2. Primary C^+, C - He collisions

We first recall that three types of SCAOCC calculations have mainly been carried out (see section 3.3): (i) a one-electron model in which a single electron of helium is active (`C+He1` and `CHe1` for C^+ and C impacts, respectively), (ii) a two-electron model with two active electrons in helium (`C+He2` and `CHe2`) and (iii) a two-electron model with one active electron in helium and another one in C^+ or C (`C+1He1` and `C1He1`).

In Figure C3(a) are reported the one-electron probabilities for projectile ionization obtained by means of the SCAOCC model (iii) for C,C^+-He collisions. These probabilities are inclusive, *i.e.* associated to all possible final states of helium. In Figure C3(b) are presented the one-electron target ionization probabilities issued from

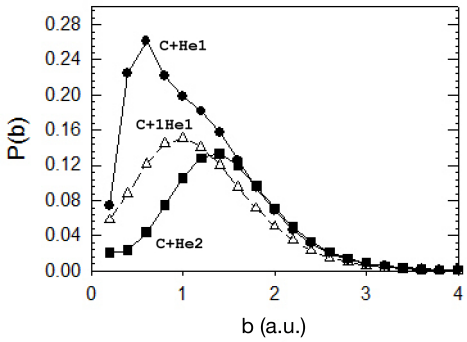

Figure C4. SCAOCC probabilities for single electron capture in C^+-He collisions at v=2.25. Circles, squares, and triangles correspond to calculations of type (`C+He1`), (`C+He2`) and (`C+1He1`) respectively (see text).

the SCAOCC model (i). Note that models (i) and (iii) are consistent with the one- and two-active-electron CTMC approaches employed to describe target and projectile ionization, respectively, in the case of Ar target. It is also worth noting that the present SCAOCC probabilities are in good agreement with CTMC calculations performed at a slightly different impact velocity (v=2 a.u.) [59]; this strenghtens the reliability of the classical CTMC approaches applied to C,C^+-Ar collisions in the present work.

We now consider electron capture. Figure C4 presents the impact parameter probabilities for C production in C^+-He collision at v=2.25. Since model (ii) explicitly takes into account the two He electrons while models (i) and (iii) do not, the single capture probability issued from (ii) has to be compared with the IPM bielectronic interpretation of single capture, *i.e.* to $2p_c(1-p_c)$ where p_c is the one-electron capture probability obtained within models (i) and (iii). This comparison, illustrated in Fig. C4, shows that two distinct capture mechanisms are at play, depending on the impact parameter: at large b, the probability (`C+He2`) closely corresponds to the probability $2p_c(1-p_c)$ issued from models (`C+He1`)and (`C+1He1`). This indicates that the electron-projectile interaction plays the major role within the capture process so that the He target can be correctly described within a mean-field (V_{mod}) approach for the electron-electron interaction. Inversely, the probabilities are strikingly different for $b \leq$1.5: in such close collisions, it is then clear that (static and dynamical) electronic correlations, whose accurate description lies beyond the mean-field V_{mod} approach, influence the collisional capture dynamics. However, the discrepancy between models is significantly reduced at the level of cross sections (see Table C1) because of the underlying integration of weighted probabilities $bP(b)$ over b.

In Figure C5 we present the probability for C^- production in C-He collisions at v=2.25. Implementations of the models (i)-(iii) have been performed, and the additional model (iv) with two active electrons on C and 1 active electron on He has further been considered (see Section 3.3). The single capture probability issued from (`CHe2`) is compared in Fig. C5 with the $2p_c(1-p_c)$ probabilities obtained with the (`CHe1`), (`C1He1`)

Table C1. SCAOCC single electron capture cross sections in C^+,C-He collisions at v=2.25. Values with asterisks were obtained from integration of IPM $2p_c(1\text{-}p_c)$ probabilities (see text)

Collision	SCAOCC type of calculations	Cross section (cm^2)
incident C^+	(`C+He1`) : frozen C^+, 1 electron on He	$6.8\ 10^{-17}$*
	(`C+He2`) : frozen C^+, 2 electrons on He	$5.0\ 10^{-17}$
	(`C+1He1`) : 1 electron on C^+, 1 electron on He	$4.8\ 10^{-17}$*
incident C	(`CHe1`) : frozen C, 1 electron on He	$3.8\ 10^{-17}$*
	(`CHe2`) : frozen C, 2 electrons on He	$2.6\ 10^{-17}$
	(`C1He1`) : 1 electron on C, 1 electron on He	$0.25\ 10^{-17}$*
	(`C2He1`) : 2 electrons on C, 1 electron on He	$0.42\ 10^{-17}$*

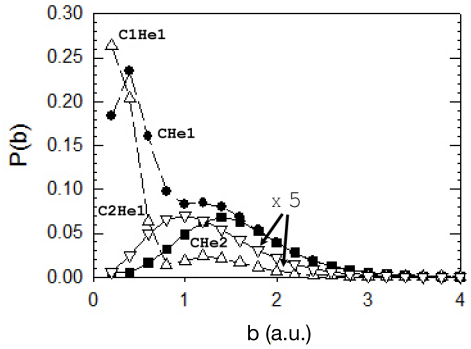

Figure C5. SCAOCC probabilities for single electron capture in C-He collisions at v=2.25. Circles, squares, triangles up and triangles down correspond to calculations of type (`CHe1`), (`CHe2`), (`C1He1`) and (`C2He1`) respectively (see text). Open triangles values (up and down) have been multiplied by a factor 5.

and (`C2He1`) models, these latter using a V_{mod} description of the electronic structure of He. As in the case of C^+-He collisions, we find a good agreement between the calculations (`CHe1`) and (`CHe2`) for b larger than 1.5 and a discrepancy for smaller b. It is not the case for model (`C1He1`) which now yields probabilities that do not match neither (`CHe1`) nor (`CHe2`) within the whole b range. The first observation leads us to conclude that an accurate description of static electron-electron correlations within the He entry channel, beyond the V_{mod} approach, is not necessary for capture at $b \geq 1.5$. However dynamical correlations, revealed by the comparison between (`CHe1`) and (`C1He1`) probabilities, strongly influence the capture process in the same b range. This was not observed in Fig. C4 for C^+-He collisions, as expected. Indeed correlations should play a larger role in C-He collisions, in which capture leads to anion formation, than in C^+-He. On the other hand, a representation of correlations leading to the correct spin multiplicity of C^- also plays a role, as revealed by the comparison of (`CHe1`) and (`C2He1`) probabilities for large b in Fig. C5. At smaller b, all kind of correlations are important in the capture process, similarly to what happened in C^+-He.

While the discrepancy between various models was not so noticeable at the level of cross sections in the case of C^+ ionic projectile, we presently find that the influence of correlations persist on the computed cross sections: models (`CHe1`) and (`C2He1`) indeed provide capture cross sections differing by a factor of about 10 (see Table C1). We checked that this difference was not originating from the opening of projectile ionization channels (obtaining similar results when closing artificially these channels in the close-coupling calculations) and attribute the difference between these two models to the role of electron correlations. Indeed the repulsion between target and projectile electrons is here probably responsible of the strong reduction of the capture cross section. Finally we note that the domains of impact parameters where electron capture occurs are pretty much the same in the case of the C^+-He and C-He collisions (see Figs. C4 and C5). This is in agreement with the CTMC calculations performed for the argon target. Moreover the range of impact parameters is not changing significantly with the level of sophistication of the SCAOCC calculations.

Finally, among the various types of SCAOCC calculations, we have retained the more sophisticated (`C+1He1`) and (`C2He1`) calculations for electron capture onto C^+ and C respectively. These probabilities are not inclusive since they are associated to electron capture without projectile ionization. In order to derive an inclusive electron capture probability we thus divided the capture probabilities respectively by $(1 - p_{\rm ion}^{(2p)})$ and $(1 - p_{\rm ion}^{(2p)})^2$. The modifications of capture probabilities induced by this division are small: their shape are almost unchanged and absolute values increased by 13% (respectively 22%) for C^+ (respectively C).